Journal of Power Sources 242 (2013) 280–288

Contents lists available at SciVerse ScienceDirect

Journal of Power Sources

journal homepage: www.elsevier.com/locate/jpowsour

Ultrahigh methanol electro-oxidation activity of PtRu nanoparticles prepared on TiO_2-embedded carbon nanofiber support

Yudai Ito, Taizo Takeuchi, Takuya Tsujiguchi, Mohammad Ali Abdelkareem, Nobuyoshi Nakagawa*

Department of Chemical and Environmental Engineering, Graduate School of Engineering, Gunma University, 1-5-1, Tenjincho, Kiryu, Gunma 376-8515, Japan

HIGHLIGHTS

- TiO_2 embedded carbon nanofiber (TECNF) is a promising support of PtRu nanocatalyst for MOR.
- PtRu/TECNF[1.0] showed 4-fold higher MOR mass activity compared to PtRu/C.
- DMFC with PtRu/TECNF[1.0] generated 2-fold higher power output with 1/4 PtRu loading.
- MOR activity of the PtRu/TECNF was maximized at the Ti/C weight ratio was 1.0.

ARTICLE INFO

Article history:
Received 3 February 2013
Received in revised form
14 May 2013
Accepted 15 May 2013
Available online 28 May 2013

Keywords:
Direct methanol fuel cell (DMFC)
Methanol oxidation reaction
PtRu nanoparticles
TiO_2 embedded carbon nanofiber
Catalyst support
Metal–support interaction

ABSTRACT

A TiO_2-embedded carbon nanofiber (TECNF) was proposed as a promising support of the PtRu nanocatalyst for the methanol oxidation reaction. The nanofiber support was prepared by the electrospinning of polyacrylonitrile (PAN) with TiO_2 nanoparticles followed by carbonization and steam activation of the nanofiber, and lastly, the PtRu nanoparticles deposition. Cyclic voltammetry (CV) revealed a significantly high MOR activity for the PtRu/TECNF compared to that of the PtRu nanoparticles deposited on different supports, i.e., carbon black (C), TiO_2 nanoparticles (TiO_2), a mixture of these nanoparticles ($C + TiO_2$) and carbon nanofiber (CNF). The MOR activity was high in the order of PtRu/TECNF > PtRu/CNF > PtRu/($C + TiO_2$) > PtRu/C >> PtRu/TiO_2. The activity of PtRu/TECNF increased with an increase in the weight ratio of Ti/C for TECNF up to 1.0 and then decreased. The MOR mass activity of PtRu/TECNF at the optimum Ti/C ratio was 4 times higher than that of PtRu/C. The ultrahigh catalytic activity of PtRu/TECNF is attributed to the metal–support interaction, which efficiently occurs at the PtRu/TECNF structure. The ultrahigh catalytic activity was also confirmed by the two-times higher DMFC power output using PtRu/TECNF, in spite of quarter the PtRu loading on the electrode, compared to that using the commercial PtRu/C.

1. Introduction

Direct methanol fuel cells (DMFCs) [1–3] have attracted much interest because of their high energy density, ease of handling of the liquid fuel and low operating temperatures. Pt and Pt-based nanoparticles have been used as a catalyst for both the oxygen reduction reaction (ORR) at the cathode and the methanol oxidation reaction (MOR) at the anode. It is well known that on the Pt catalyst at the anode, CO as an intermediate adsorbate during the methanol oxidation strongly adsorbs on the surface, and it causes catalyst poisoning. The MOR is preferentially catalyzed on bimetallic catalysts [4–9], such as PtRu [6–9], which promote the CO tolerance and increase the catalytic activity according to the bifunctional mechanism [6,7]. However, the improved MOR activity of PtRu is still not sufficient for practical use. The power output of the DMFC is usually much lower than that of the hydrogen fuel cell with a polymer electrolyte, and hence, more than ten times a higher loading of the precious metal catalyst is necessary for the DMFC to achieve a comparable power output to that of the hydrogen fuel cell. The high cost for the high amount of the precious metals and the insufficient activity hinder the DMFC from commercialization. Hence, enhancement of the catalyst activity and reduction of the precious metal loading are major efforts in current DMFC research.

* Corresponding author. Tel.: +81 277 30 1457; fax: +81 277 30 1458.
E-mail addresses: nakagawa@cee.gunma-u.ac.jp, nobnaka@sannet.ne.jp (N. Nakagawa).

0378-7753/$ – see front matter © 2013 Elsevier B.V. All rights reserved.
http://dx.doi.org/10.1016/j.jpowsour.2013.05.064

The Pt and Pt-based catalysts are usually used by being homogeneously dispersed and deposited on a support material such as various types of carbons [10–17] and other materials [17] mainly to keep the increased specific surface area of the nanoparticles and avoid agglomeration. The selection of the support is of key importance for the catalytic activity and durability [17–21]. The metal oxides have become attractive as alternative catalyst supports due to their excellent chemical stability under acidic and oxidative conditions and also their specific positive effect on the activity.

It is widely known that Pt and Pt-based nanoparticles on a TiO_2 support [18,20,22–37] show enhanced catalytic activities for the MOR and ORR due to a metal–support interaction of which the mechanism has not yet been identified. The quantum mechanical calculations suggested that TiO_2 increased the electron density on Pt and changes its chemisorptive properties for the intermediates, and then, it decreases the energy of the Pt–CO bonding and the activation energy of the CO_{ad} surface mobility [32]. TiO_2 may provide a highly reactive oxygen species like OH to the active sites [24,30–34] and promote the CO oxidation. A positive correlation between the enhanced catalytic activity and the proton spillover effect [38–40] was also observed at a Pt/TiO_2 electrode [31]. These would be related to the interaction of the metal–support system in this case.

On the other hand, for the fuel cell, a high electric conductivity of the support is necessary for the catalyst and the support in order to efficiently collect and transport electron. However, TiO_2 is a semiconducting material of which the electric conductivity is quite low for the conditions of the fuel cell operation, thus this is a disadvantage in using TiO_2 as the support of the metal electrocatalyst [22]. To overcome the low electric conductivity of TiO_2, high loadings of the Pt catalyst over the TiO_2 support [22], composite with an electric conducting material such as carbon [23–27,33], Nb-doping [22,26,36] and employment of substoichiometric titanium oxide [35] have been proposed. The mixtures of TiO_2 nanoparticles with Pt/C [24,25,27,33,37] and carbon-coated TiO_2 [26] have been already demonstrated showing an instant effect on the catalytic activity for the oxidation reaction of methanol and ethanol. However, such a composite structure of the nanoparticle mixture is not very effective to derive a sufficient electrical conduction between the particles based on the point contacts, and the carbon coating reduces the extent of the Pt/TiO_2 interface by covering the surface of the TiO_2 with carbon. In both cases, the promoting effect by the metal–support interaction would be limited. A closer connection between the TiO_2 nanoparticles and electro conductive media is a key issue to compensate for the low electrical conductivity of the TiO_2. We propose a TiO_2 embedded carbon nanofiber as the support for Pt-based nanoelectrocatalysts by which an increased electronic conduction, from the reaction sites on the metal nanoparticles to the current collector through the support and the catalyst layer, and hence, the promoted fuel cell performance.

In this study, TiO_2 embedded carbon nanofibers, TECNF, were proposed as a promising support of the PtRu nanoelectrocatalyst for the methanol oxidation reaction. The nanofiber support was prepared by electrospinning [41,42] using polyacrylonitrile (PAN) with the commercial TiO_2 nanoparticles followed by carbonization and steam activation of the nanofibers, and lastly the PtRu nanoparticle deposition. X-ray diffraction (XRD), energy dispersive X-ray spectroscopy (EDX), field emission scanning electron microscopy (FE-SEM) and transmission electron microscopy (TEM) were used to characterize the prepared catalysts. The MOR activity for the PtRu/TECNF was evaluated by cyclic voltammetry using a glassy carbon electrode and compared to that for PtRu nanoparticles prepared on different supports including carbon black, TiO_2 nanoparticles, CNF without TiO_2 addition and a mixture of carbon black and TiO_2 nanoparticles. As a sensitive factor, the effect of the TiO_2 content in TECNF on the MOR activity was investigated by conducting CO stripping voltammetry to evaluate the electrochemically active surface area (ECSA). Using the PtRu/TECNF with the optimized Ti/C ratio, the DMFC power generation was also tested and compared to that using a commercial PtRu/C catalyst. Based on the experimental results, the effects of the composite structure of the different supports and the TiO_2 composition of the TECNF support on the catalytic activity are discussed.

2. Experimental

2.1. Catalyst preparation

2.1.1. Preparation of the TiO_2 embedded carbon nanofiber support

All the reagents used in this study were of analytical grade if not specified. Polyacrylonitrile (PAN, Sigma–Aldrich Co., Ltd.) was used as the carbon source of the nanofibers. The PAN solution was prepared by dissolving it into dimethylformamide (DMF, Wako Pure Chemicals Ind., Ltd.) by stirring the solution at 60 °C for 1 h followed by stirring overnight at room temperature. A certain amount of high purity TiO_2 nanoparticles of 80% anatase and 20% rutile (P25, Nippon Aerosil Co., Ltd.) was added to the PAN solution and the mixture was then stirred for 2 h. Different mixtures of different weight ratios of the TiO_2 to PAN were prepared. The mixed solution containing the TiO_2 nanoparticles was transferred to a glass syringe attached to a stainless needle for the electrospinning.

Electrospinning of the precursor mixture was conducted by applying 16 kV between the needle and a metallic collector covered with aluminum foil at a distance of 18 cm between them and feeding the precursor mixture at 0.05 mL min^{-1} into the electric field. A high voltage power supply (Pulse Electronic Engineering Co., Ltd.) with the maximum voltage of 50 kV was used to apply the high voltage, and a syringe pump (Future Science Co., Ltd.) was used to control the solution feed rate. The nanofiber sheet formed on the collector was initially dried in air for 3 h at room temperature and then stabilized by heating at 250 °C in air for 10 h. The stabilized nanofibers were carbonized in a tube reactor with a 30-mm diameter, placed in an electric furnace, then heated at 1000 °C for 1 h in a nitrogen atmosphere. Unless otherwise noted, the carbonized nanofibers were then treated with steam at 850 °C for 1 h by introducing N_2 after bubbling in water at 70 °C into the tube reactor at 200 mL min^{-1}. The obtained nanofibers were then milled using an agate mortar for 5 min per 200 mg of the nanofibers to normalize the fiber length. The TiO_2 embedded carbon nanofiber by the steam treatment is denoted TECNF with the weight ratio *x* (=Ti/C) on the abscissa like TECNF[*x*].

2.1.2. PtRu nanoparticle deposition

The 20 wt% Pt–Ru (in an atomic ratio of 1:1) was deposited on the TECNF and the other support materials including the carbon black (Vulcan XC-72R, C), TiO_2 nanoparticles (P25, TiO_2) and the mixture of these particles (C + TiO_2) by the chemical reduction with $NaBH_4$ (Wako Pure Chemicals Ind., Ltd.) of H_2PtCl_6 (Wako Pure Chemicals Ind., Ltd.) and $RuCl_3$ (Wako Pure Chemicals Ind., Ltd.) as the precursor. The support material was ultrasonically dispersed in a mixture of distilled water and isopropyl alcohol for 20 min. The precursors of Pt and Ru were then added to the mixture followed by stirring for 20 min. The pH value of the mixed solution was adjusted with a NaOH solution to 8 and then its temperature was raised to 80 °C. Twenty-five milliliters of a 0.2 M solution of $NaBH_4$ was added drop by drop to the mixture with stirring for 1 h. The mixture was cooled, dried and repeatedly washed with distilled water. The catalyst powder was finally dried for 3 h at 120 °C.

2.2. Characterization of the catalyst

The surface morphology and elemental analysis of the prepared catalysts were studied by FE-SEM (JSM-6330F, JEOL, Ltd.) and EDX (EX-200K, Horiba, Ltd.), respectively. A high-resolution image of a selected area was also observed by a JEOL 2010 transmission electron microscope (TEM) operating at 200 kV with EDX (Oxford Instrument, Ltd.). The crystal structures of the prepared PtRu catalyst on the different supports were investigated based on the X-ray diffraction (XRD) patterns for the powder samples using an X-ray diffractometer (RINT2100/PC, Rigaku Corp.). The X-ray source was Cu-Kα operating at 32 kV and 20 mA.

2.3. Evaluation of the catalytic activity

The MOR activities of the prepared catalysts with the different supports were determined by measuring the cyclic voltammetry in a three-electrode cell with a fixed glassy, carbon electrode (GCE) (3-mm diameter) at room temperature. The catalyst ink was prepared by dispersing 5 mg of the catalyst in a mixture containing 80 μL of water, 80 μL of ethanol, and 25 μL of a 5 wt% Nafion solution (Wako Pure Chemicals Ind., Ltd.), then the mixture was ultrasonicated for 30 min. A 2.5 μL aliquot of the ink was removed using a micropipette and deposited on the glassy carbon electrodes. After the electrode was dried at room temperature in air for 1 h, it was heated in an oven at 100 °C for 30 min. A Pt wire and a mercury/mercurous sulfate electrode were used as the counter and reference electrodes, respectively. The electrolyte was a solution of 2 M methanol containing 0.5 M H_2SO_4. After nitrogen was bubbled into the solution for 20 min to obtain an oxygen-free atmosphere near the working electrode, the CV measurement was conducted in the potential range from 0 to 1.2 V vs. NHE at the scan rate of 20 mV s^{-1} during N_2 bubbling at room temperature.

Some of the PtRu catalysts supported on the TECNF[x] with different x values were evaluated by CO stripping voltammetry. The CO stripping experiments were conducted using the following procedures: (i) N_2 (100 mL min^{-1}) was bubbled into the 0.5 M H_2SO_4 solution for 30 min; (ii) He containing 10% CO was bubbled for 30 min while keeping the potential at −0.3 V vs. NHE for the CO adsorption; (iii) N_2 (100 mL min^{-1}) was bubbled again for 30 min to remove any traces of dissolved CO; (iv) five cyclic voltammetries (CV) were successively performed at the scan rate of 10 mV s^{-1} from 0.3 to 0.8 V vs. NHE for the CO oxidation during the first cycle, and from 0 to 0.8 V vs. NHE during the subsequent cycles to record the base CV.

The measurements were conducted using an electrochemical measurement system (HAG-5010, Hokuto Denko, Co., Ltd.). The activity of the prepared catalyst was expressed based on the total amount of the Pt and Ru on the glassy carbon electrode.

2.4. MEA preparation and DMFC operation

The DMFC performance of the membrane electrode assembly (MEA) with the different prepared anode catalysts was evaluated. A certain amount of the catalyst was painted on the carbon paper (TGP-H-090, Toray) in the form of a slurry with 2-propanol and water. This was then used as the anode after drying. The electrolyte membrane, Nafion117 (Du Pont), was sandwiched between the anode and a commercially available Pt (1.0 mg cm^{-2})/C electrode (EC-20-10, ElectroChem, Inc.) as the cathode by hot pressing them at 410 K, 5 MPa, for 3 min to obtain the MEA. The MEA with the commercial PtRu/C (TEC61E54, Tanaka Kikinzoku Kogyo K.K., Pt: 30.0 wt%, Ru: 23.3 wt%) as the anode was also prepared by a similar procedure and used for comparison. The MEA was fixed in the cell block with serpentine flow channels in both the anode and cathode (FC05-01SP, ElectroChem, Inc.), and was operated by pumping a 2 M aqueous methanol solution at 1.5 mL min^{-1} to the anode and feeding dry oxygen or air to the cathode at 353 K. The current voltage, i–V, curve and time of the current density at a constant cell voltage were measured for each MEA. The measurements were also conducted using the electrochemical measurement system (HAG-5010, Hokuto Denko, Co., Ltd.).

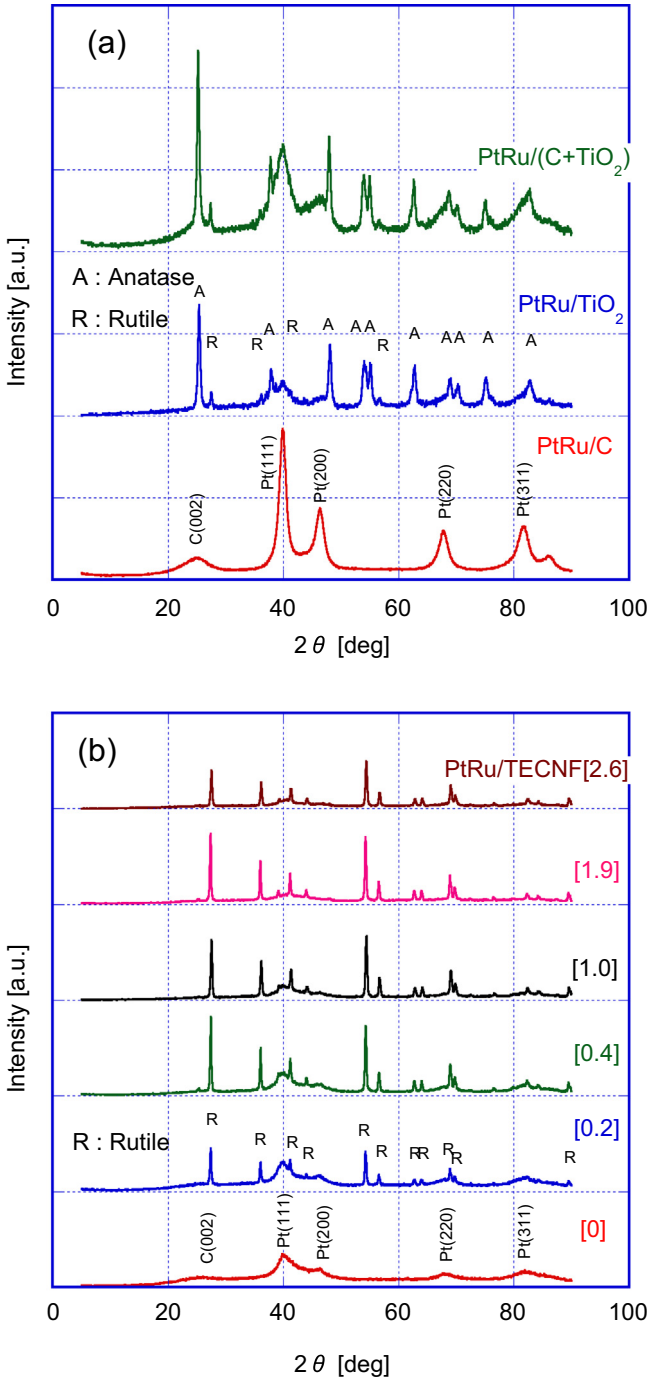

Fig. 1. X-ray diffraction patterns for the catalysts prepared in this experiment. (a) PtRu supported on carbon black (C), TiO_2 nanoparticles (TiO_2) and the mixture of these nanoparticles (C + TiO_2), (b) PtRu supported on TiO_2-embedded carbon nanofibers (TECNF[x]) with different x = Ti/C values.

3. Results and discussion

3.1. Characteristics of the catalyst

Fig. 1 shows the XRD patterns of the PtRu catalyst deposited on the different supports; PtRu on the carbon black (PtRu/C), TiO_2 nanoparticles (PtRu/TiO_2), and on the mixture of these powders (PtRu/(C + TiO_2)) in Fig. 1(a), and PtRu on TECNF with different Ti/C ratios, x, (PtRu/TECNF[x]) in Fig. 1(b). Peaks for the carbon, Pt and TiO_2 anatase and/or rutile were detected; both the rutile and anatase were from PtRu/TiO_2 and PtRu/(C + TiO_2) in Fig. 1(a), whereas, only rutile was from PtRu/TECNF[x] in Fig. 1(b). The anatase in the raw TiO_2 particles (P25) was transformed into rutile due to the high temperature carbonization treatment at 1000 °C for 1 h. Almost no influence of the Ti/C ratio on the crystal structure of the TiO_2 and PtRu was found in the figure. For the PtRu particles, broad peaks appeared, except for PtRu/C, showing a face-centered cubic structure; a slight shift in the peak position for Pt(111), 40.1° ± 0.1° (=2θ), from that of pure platinum, 39.76°, was related to the Ru alloying effect [24]. The crystalline size, d, of the PtRu and TiO_2 was calculated by the width of the peak at half height for the Pt(111) at 40° and TiO_2(101) at 27.5°, respectively, using Scherrer's equation.

$$d = 0.9\lambda/\beta\cos\theta$$

where λ is the wavelength of the X-ray (1.54056 Å), θ is the angle at the peak, and β is the width of the peak at half-height. The crystalline size of PtRu was calculated to be 4–9 nm, although a relatively large error may be included due to the broadening of the peak, and that of TiO_2 was between 30 nm and 70 nm as summarized in Table 1. Relatively smaller sizes, between 3.5 nm and 5.1 nm, of PtRu were obtained for the TECNF support compared to that for the carbon black and its mixture, 5.5 nm–9.4 nm, which may be due to the effect of the N-doped carbon, of the TECNF as revealed later, on which the smaller size of the Pt and Pt-alloy particles are obtained [21] and due to TiO_2.

The compositions of the prepared catalysts analyzed by EDX for the SEM viewing field at a 3500 magnification are also listed in the table as an average value of the three measurements. As an example, one of the corresponding EDX spectra for the composition of PtRu/TECNF[1.0] is shown in Fig. 2. The Pt to Ru atomic ratio was about 1.0, the PtRu loading was about 20 wt%, and they were almost the same in the prepared catalyst.

The above measurements revealed that similar PtRu nanoparticles in the loading and in the Pt/Ru ratio had been successfully prepared on the different supports.

Fig. 3 shows the FE-SEM pictures taken for TECNF and PtRu/TECNF with different Ti/C ratios. The TECNFs in Fig. 3(a) and (b)

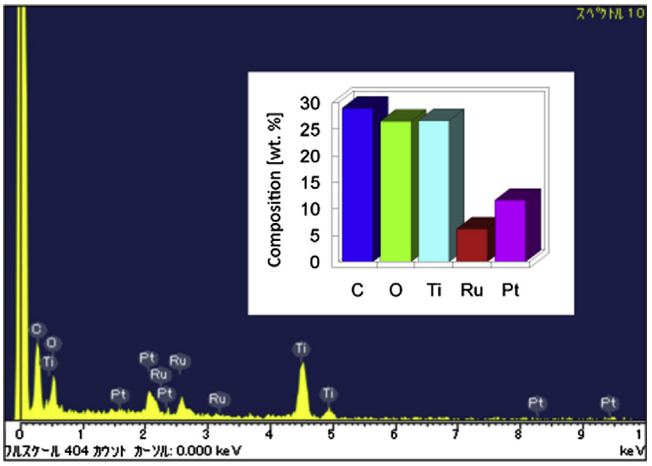

Fig. 2. EDX spectra for PtRu/TECNF[1.0] (the analysis was conducted for the SEM viewing field at 3500 magnification).

were observed before milling of the obtained nanofibers, hence, long fiber structures of 100–300 nm diameter were maintained in both cases. However, in Fig. 3(b) in which the Ti/C ratio was as high as 2.6, many bare white particles, TiO_2 particles and their agglomerates, attached on the thin fiber could be seen, whereas the TiO_2 particles were embedded in the nanofibers at the low Ti/C ratio, 0.9, in Fig. 2(a). Fig. 3(c)–(e) are the pictures taken after the milling and the PtRu deposition. Short fiber structures were observed at the low Ti/C ratios, 0.2 for (c); PtRu/TECNF[0.2], and 1.0 for (d); PtRu/TECNF[1.0]. On the other hand, beaded particles were observed at the high Ti/C ratio of 2.6, (e); PtRu/TECNF[2.6], which resulted from separation of the TiO_2 particles from the fibers by the milling of the thin fibers is shown in Fig. 3(b). In Fig. 3(c) and (d), TiO_2 particles, the white particles with a 100 nm or less size, exposed on the fiber surface can be significantly seen on PtRu/TECNF[1.0], but not much on PtRu/TECNF[0.2]. The FE-SEM observations revealed the difference in shapes, short fiber or beaded particles, and the different number of TiO_2 particles on the support at the different Ti/C ratios.

Fig. 4(a) and (b) show the TEM images of PtRu/TECNF[1.0] and PtRu/TECNF[0.2], respectively. In Fig. 4(a), the many TiO_2 particles with 30–70 nm sizes, the black circles, that correspond to those from the XRD analysis were homogeneously embedded in the carbon nanofiber with a 300 nm diam. On the other hand, in Fig. 3(b), the number of the TiO_2 particles was very low. These are in accordance with the SEM images shown in Fig. 3(c) and (d). It was observed, in Fig. 4(b), that the PtRu particles with about 5 nm were deposited on both of the CNF and the exposed TiO_2 surfaces. The

Table 1
Properties of the PtRu catalyst with the different supports measured with XRD and EDX.

Catalyst	Composition [wt%]					Pt/Ru [atm/atm]	Ti/C [wt/wt]	PtRu crystalline size [nm]	TiO_2 crystalline size [nm]
	Pt	Ru	C	Ti	O				
PtRu/C	10.2	5.7	84.2	–	–	0.93	–	9.4	–
PtRu/TiO_2	12.2	5.1	–	39.3	43.5	1.23	–	5.5	32.2
PtRu/(C + TiO_2)	9.8	5.3	55.0	13.0	16.9	0.95	0.24	6.7	40.2
PtRu/TECNF[0]	13.4	6.9	70.4	–	9.3	1.01	0.00	5.0	–
PtRu/TECNF[0.2]	13.8	7.3	57.4	9.7	11.9	0.98	0.17	5.1	62.2
PtRu/TECNF[0.4]	11.2	6.4	46.5	18.0	17.9	0.90	0.39	4.5	71.4
PtRu/TECNF[0.9]	10.2	6.6	30.8	27.2	25.3	0.80	0.88	–	–
PtRu/TECNF[1.0]	12.9	7.4	27.4	28.5	24.3	0.87	1.04	3.5	54.7
PtRu/TECNF[1.9]	10.7	7.6	18.8	35.5	27.4	0.73	1.89	3.9	71.4
PtRu/TECNF[2.6]	11.5	6.4	13.7	36.0	33.0	0.94	2.62	6.4	59.3
PtRu/C_{com}	30.0	23.3	46.7	–	–	1.29	–	7.7	–

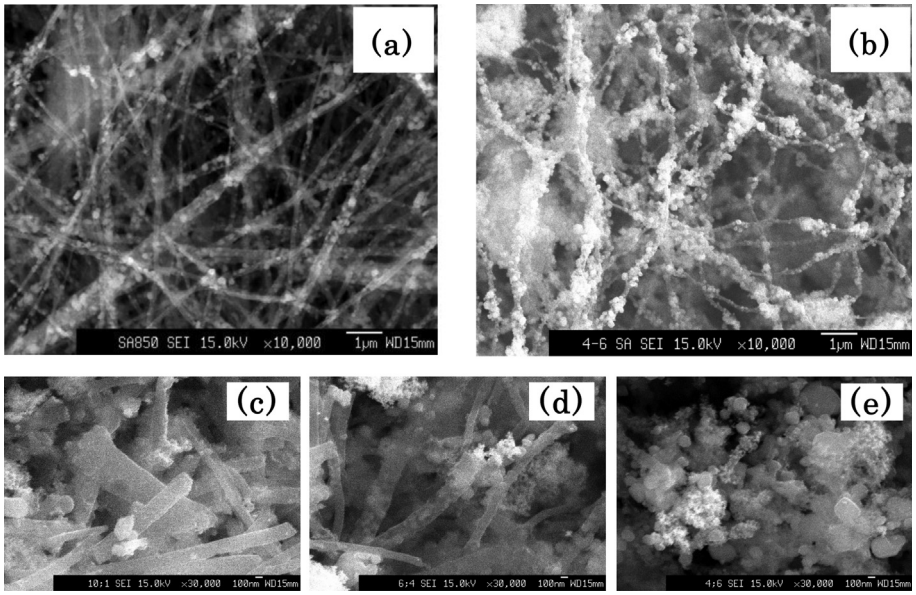

Fig. 3. FE-SEM images for TECNF obtained after steam activation, (a) TECNF[0.9], (b) TECNF[2.6], and that for PtRu/TECNF as the catalyst, (c) PtRu/TECNF[0.2], (d) PtRu/TECNF[1.0], and (e) PtRu/TECNF[2.6].

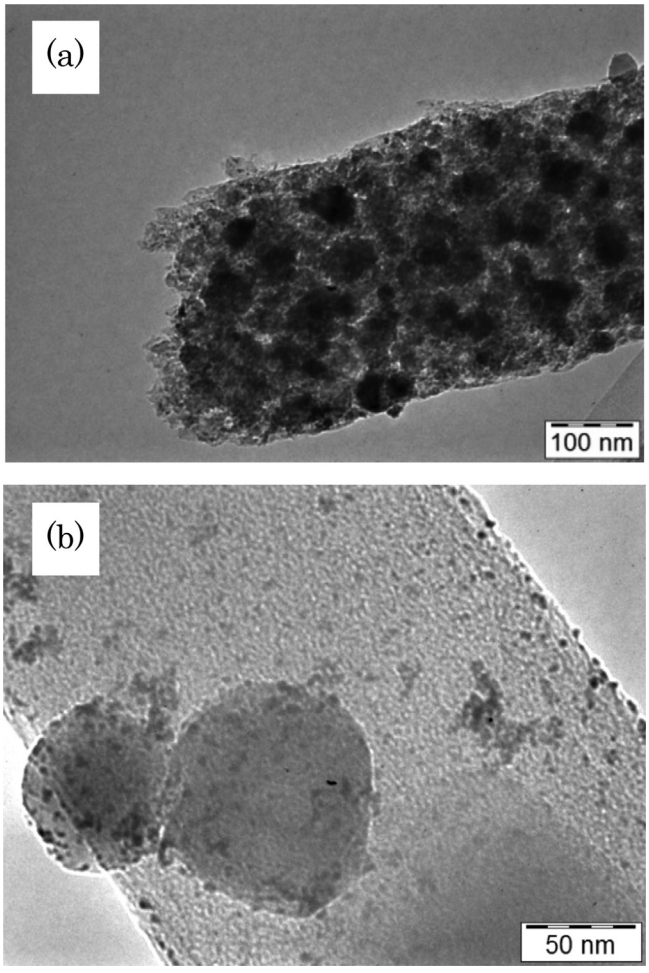

Fig. 4. TEM images of PtRu/TECNF[1.0], (a), and PtRu/TECNF[0.2], (b), prepared.

PtRu particles were not homogeneously dispersed on the surfaces, and agglomerates with 20 nm or larger sizes could be seen.

Based on the FE-SEM and TEM observations, the close connection between the TiO_2 nanoparticles and the carbon of the fiber was confirmed for the PtRu/TECNF[x]s with the relatively low x values, including $x = 0.2$, 0.9 and 1, due to the TiO_2 embedding on the carbon nanofiber.

3.2. Methanol oxidation activity for the catalysts with the different supports

Fig. 5 shows the CV curves measured in 2 M methanol with 0.5 M H_2SO_4 at room temperature for the catalysts with the different supports; PtRu/C, PtRu/TiO_2 and PtRu/CNF (PtRu/TECNF[0]) in Fig. 5(a), and PtRu/(C + TiO_2) and PtRu/TECNF[0.2] in Fig. 5(b). In Fig. 5(a), the peak current density for the MOR appeared around 0.9 V vs. NHE and was high in the order of PtRu/CNF > PtRu/C >> PtRu/TiO_2. The very low activity of PtRu/TiO_2 could be attributed to the low electric conductivity of the TiO_2 support. It was clear that an electro conductive medium is indispensable for the PtRu/TiO_2 system when it was used as the catalyst for the electrochemical reaction. The higher activity of the PtRu/CNF compared to PtRu/C can be explained by the advantages of the macro-structured catalyst layer, which has fewer incidences of agglomeration, high specific volume, and high electro- and thermal conductivities. Another advantage may be pointed out for the promoted activity by the N-doped carbon of the support, CNF (TECNF[0]). It was reported that the N-doped carbon support enhances the MOR activity of the Pt and Pt-based catalysts [10,21,26,43] and the durability [43]. Actually, the X-ray photoelectron spectroscopy of the CNF (TECNF[0]) surface detected about 0.8 atomic percent N from PAN used as the carbon source, although the EDX did not detect it. The CNF (TECNF[0]) was clearly a better support for the catalyst than the carbon black (Vulcan XC-72R). In Fig. 5(b), the PtRu nanoparticles on the carbon–TiO_2 composite support with the different structures were compared. A significantly high, about 2 times higher, peak current density, i.e., mass activity, was obtained from the catalyst with the TECNF support compared to that with the (C + TiO_2) support under similar Ti/C

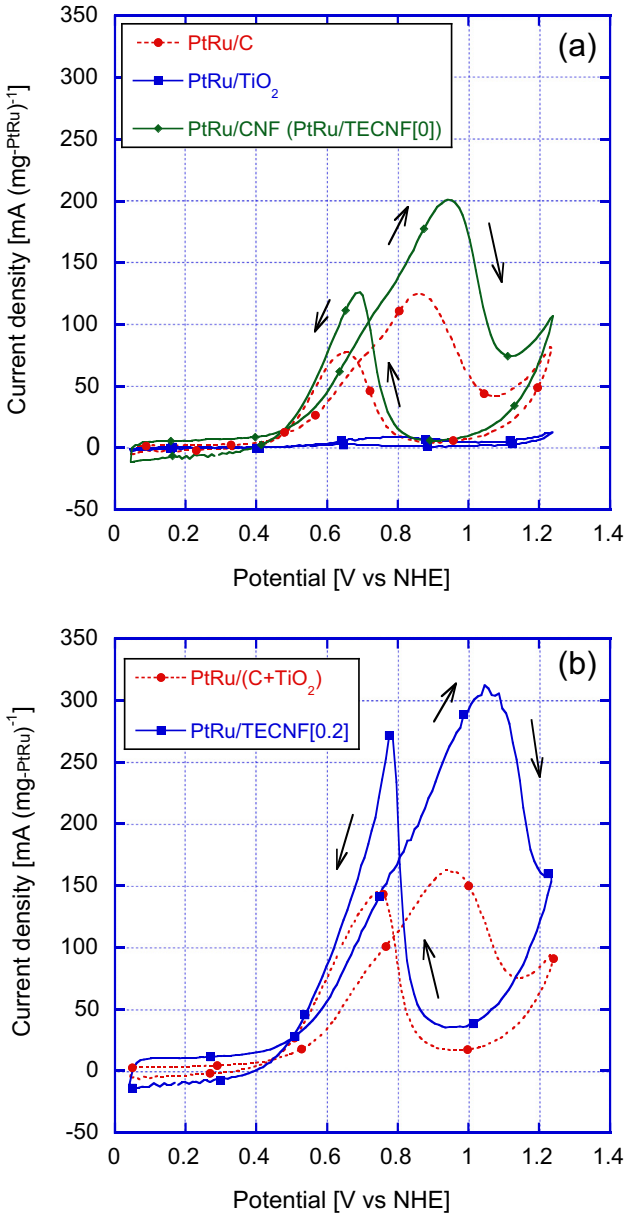

Fig. 5. Cyclic voltammograms for the PtRu catalysts prepared on different supports measured in 2 M methanol with 0.5 M H_2SO_4 at the scan rate of 20 mV s^{-1}. (a) PtRu/C, PtRu/TiO_2, and PtRu/CNF (=PtRu/TECNF[0]), (b) PtRu/(C + TiO_2); Ti/C = 0.24 and PtRu/TECNF[0.2]; Ti/C = 0.17.

conditions, $x = 0.2$. When the crystal structures of TiO_2, anatase and rutile, were compared as the support of the catalyst for the alcohol oxidation activity, anatase exhibited a much higher activity than the rutile [22]. In contrast, the results in Fig. 5(b) indicated the superior performance of the catalyst having the TECNF support with rutile than that with (C + TiO_2) of which the TiO_2 was mainly anatase as shown in Fig. 1. This suggested that the TiO_2 embedded carbon nanofiber is a superior structure to take advantage of using the composite of TiO_2 and carbon as the support for the Pt and Pt-alloy nanoparticles. Additionally, the TECNF prepared in this study may have the advantage of the N-doped carbon and the disadvantage of using rutile TiO_2 related to the MOR activity. Based on the peak current density shown in Fig. 5(a) and (b), the catalytic activity for the different supports was high in the order of PtRu/CTNF[0.2] > PtRu/CNF > PtRu/(C + TiO_2) > PtRu/C >> PtRu/TiO_2. The highest peak current density for PtRu/TECNF was clearly attributed to the TiO_2 embedded CNF support.

The onset potential for the MOR at which the current rises from the horizontal curve in the low potential region, the peak current density and the peak position obtained from the figure are summarized in Table 2. Except for PtRu/C, there was a trend in the lower onset potential for the higher peak current density. For the peak position, a relatively high difference was observed among the different catalysts, i.e., 0.85 V, 0.94 V, 0.94 V and 1.05 V vs. NHE for PtRu/C, PtRu/(C + TiO_2), PtRu/CNF and PtRu/TECNF[0.2], respectively. The higher peak potential for the TECNF support may be due to the IR drop of the catalyst layer with the relatively low electric conductivity of the fiber prepared on the glassy carbon plate [44], although we do not have clear evidence for it.

Based on the previous results, one can clearly understand the advantage of TiO_2 embedding in carbon and that of using nanofiber supports. The TiO_2 content, which is a sensitive factor for the activity, will be discussed in the next section.

3.3. Effect of the Ti/C ratio of TECNF on the mass activity for the MOR

In order to investigate the effect of the TiO_2 content in the TECNF support on the activity, a series of catalysts with different Ti/C weight ratios (=x) was prepared, and all the MOR activities were compared. Fig. 6 shows the CV curves measured in the methanol solution for the PtRu/TECNFs with different x values from 0 to 2.6. The obtained onset potential for the MOR, the peak current density and the peak position are summarized in Table 2. The peak current density, mass activity, for the methanol oxidation increased with the increasing x to 1.0 and then decreased. PtRu/TECNF[1.0] exhibited the highest mass activity of the peak current density of 516 mA $(mg_{\text{-PtRu}})^{-1}$, and it was 2.6 and 4.2 times higher than that of PtRu/CNT and PtRu/C in Fig. 5(a), respectively. Such a large change of 4.2 times based on the activity of PtRu/C is superior to that previously reported, i.e., the nanoparticle TiO_2-promoted PtRu/C (1.2 times) [27], PtRu/C–Au/TiO_2 (1.7 times) [28], PtRu/Nb–TiO_2 (2.2 times) [22], and PtRu/TiO_2–C (2.7 times) [29]. This suggests that PtRu/TECNF is a very effective structure to effectively produce the metal–support interaction. The Ti/C ratio is related to the extent of the TiO_2 exposed surface that may be important for the metal–support interaction. Hence, a higher MOR activity was expected with the increase in the Ti/C ratio, x value. The suppressed activity at the higher Ti/C ratio over 1.0, $x > 1.0$, would be due to the change in the support structure from fibers to beads as shown in Fig. 3(e). In the beads structure, a good electron conduction through the catalyst layer would not be expected, and separation of TiO_2 particles from the CNF would also reduce the interaction.

Table 2
Summary of the catalysts with the different supports in terms of onset potential, peak current density and peak potential from the CV curve for MOR.

Catalyst	Onset potential [V vs. NHE]	Peak potential, E_p [V vs. NHE]	Mass activity at E_p, $i_{p\text{-MOR}}$ [mA $(mg_{\text{-PtRu}})^{-1}$]	Mass activity, relative value [-]
PtRu/C	0.346	0.85	125	0.62
PtRu/TiO_2	0.478	0.81	9	0.04
PtRu/(C + TiO_2)	0.373	0.94	162	0.81
PtRu/TECNF[0]	0.350	0.94	202	1.00
PtRu/TECNF[0.2]	0.350	1.05	313	1.55
PtRu/TECNF[0.4]	0.338	1.01	366	1.81
PtRu/TECNF[0.9]	0.319	0.95	406	2.01
PtRu/TECNF[1.0]	0.310	1.06	516	2.55
PtRu/TECNF[1.9]	0.315	1.00	451	2.23
PtRu/TECNF[2.6]	0.346	0.89	202	1.00

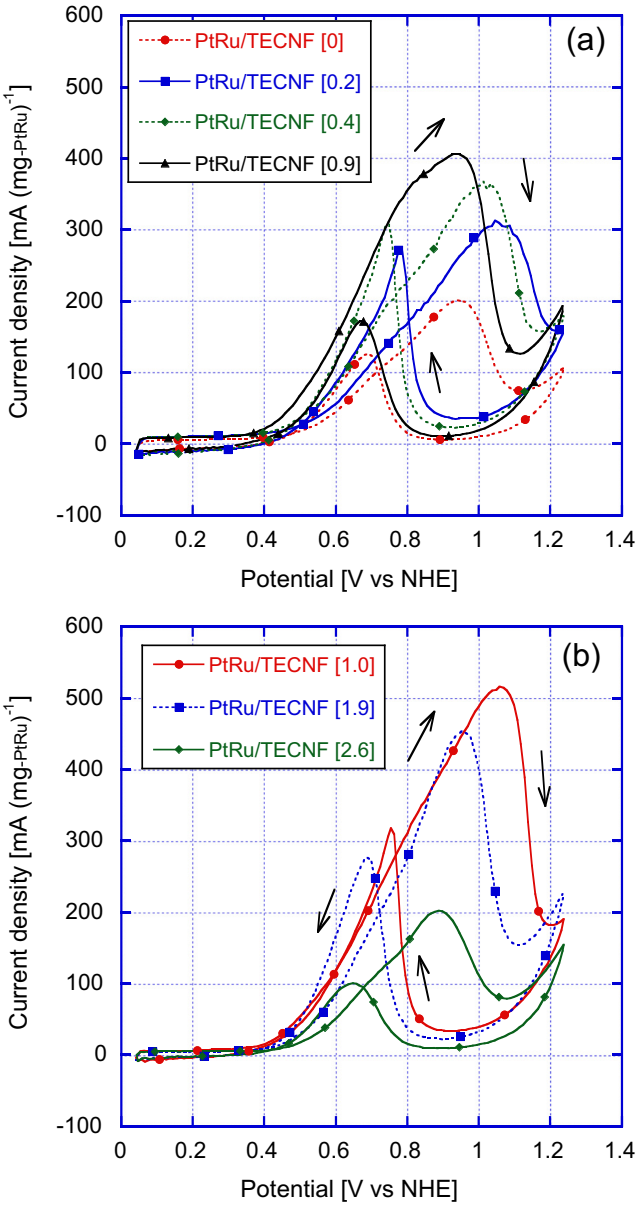

Fig. 6. Cyclic voltammograms for PtRu/TECNF with different Ti/C ratios measured in 2 M methanol with 0.5 M H_2SO_4 at the scan rate of 20 mV s^{-1}. (a) PtRu/TECNF[x]; x = 0–0.9, (b) PtRu/TECNF[x]; x = 1.0–2.6.

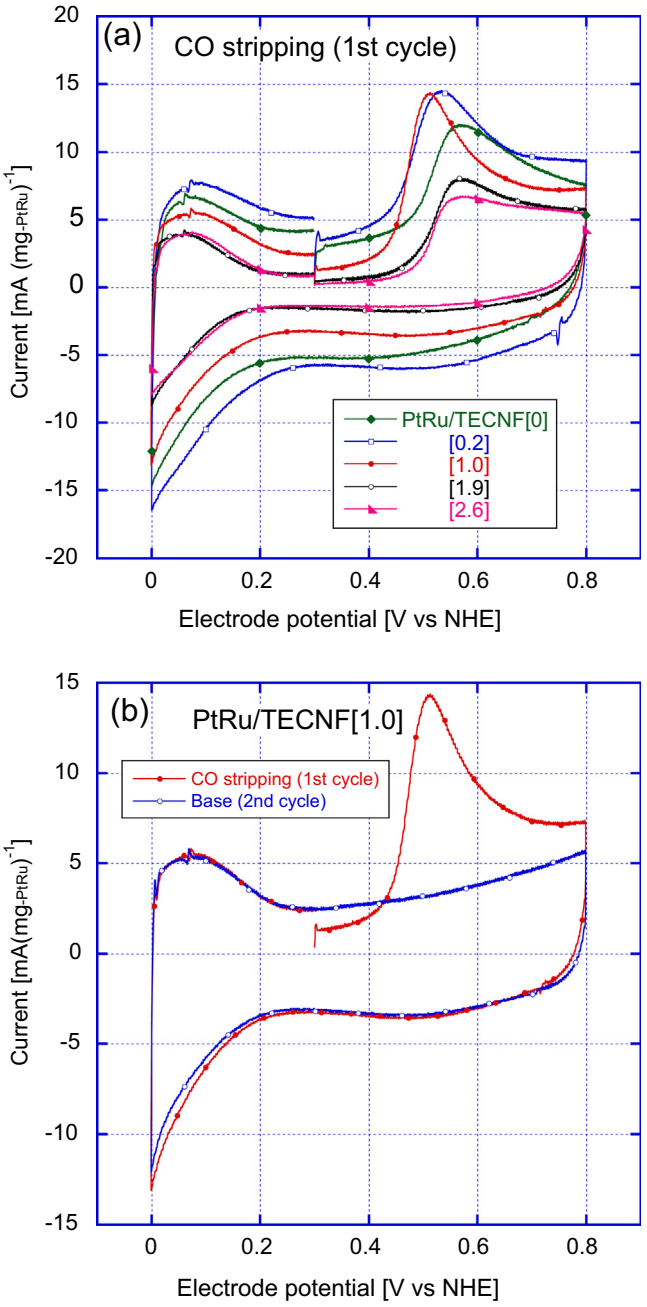

Fig. 7. The CO stripping voltammograms for the PtRu/TECNF[x]s (x = 0, 0.2, 1.0, 1.9 and 2.6) (a) and the first two cycles of CVs for the PtRu/TECNF[1.0] (b) in 0.5 M H_2SO_4 solution with a scan rate of 10 mV s^{-1}. CO adsorption was conducted at a fixed potential of 0.3 V vs. NHE in 0.5 M H_2SO_4 solution with 10% CO bubbling for 30 min after N_2 (100 mL min^{-1}) bubbling into the solution for 30 min, and then N_2 (100 mL min^{-1}) was bubbled again for 30 min.

Based on the above discussion, the optimum TiO_2 content was determined. The optimum content was the maximum in the content range in which the nanofiber structure was maintained for the support.

3.4. CO stripping voltammetry for PtRu/TECNF with the different TiO_2 contents

In order to investigate the reason for the increased activity, the electrochemically active surface area (ECSA) was evaluated by the CO stripping voltammetry for some of the PtRu/TECNF[x] samples. Fig. 7(a) shows the CO stripping voltammograms for the PtRu/TECNF[x]s (x = 0, 0.2, 1.0, 1.9, 2.6). One can note the variation in the double layer capacitance, which corresponds to the difference in the potentials for the forward scan and for the backward scan at the potential where the CV curve became horizontal, at around 0.25 V. The double layer capacitance decreased with the increase in x except for the case of x = 0.2, although the reason for this is not clear at the time.

The peak potential for the CO stripping was dependent on the value of x, and it decreased with the increase in x up to x = 1.0 and then increased. The lowest peak potential at x = 1.0 was 0.516 V vs. NHE, and it was almost 0.06 V lower than that of PtRu(1:1)/C from previous reports [8,12]. The low and Ti/C dependent potentials suggest the effect of the metal–support interaction that enhances the MOR activity.

ECSA of the catalysts was measured using the CO oxidation charge after subtracting the base current of the subsequent CV curve as shown in Fig. 7(b), although only the case of $x = 1.0$ is shown here, by assuming 420 μC cm^{-2} as the oxidation charge for one monolayer of CO on a smooth Pt surface. The measured ECSA values and the peak potentials are summarized in Table 3. The relative values of ECSA and the relative mass activity based on the values for $x = 0$ are also listed in the table for the quantitative consideration of the effect of Ti/C ratio on the MOR activity. The ECSA values measured for the PtRu/TECNF[0], PtRu/TECNF[0.2] and PtRu/TECNF[1.0] were 342 m^2 ($g_{\text{-PtRu}}$)$^{-1}$, 354 m^2 ($g_{\text{-PtRu}}$)$^{-1}$ and 427 m^2 ($g_{\text{-PtRu}}$)$^{-1}$, respectively, showing significantly high values that are 3–5 times greater than that obtained for the PtRu(1:1)/C in previous reports [8,12]. The ECSA increased with the increase in x up to $x = 1.0$ and then decreased. When the increase in ECSA from $x = 0$ to 1.0, about a 25% increase, is compared to the increase in the calculated geometric surface area based on the PtRu crystalline size in Table 1, the 25% increase of ECSA may seem to be low. This small increase in ECSA would be due to agglomeration of the PtRu particles as observed in Fig. 3(b). For the catalysts with $x > 1.0$, the nanofiber structure of the support was destroyed as shown in Fig. 3(e), and then the ECSA would decrease. The metal–support interaction was maximized at $x = 1.0$ when the TiO_2 content in the carbon nanofiber became a maximum along with keeping the nanofiber structure for the support.

As shown in Table 3, the value of the relative mass activity for each PtRu/TECNF[x] ($x > 0$) was greater than that of the relative ECSA. For example, the most active catalyst, PtRu/TECNF[1.0], showed the relative mass activity of 2.55 that is more than 2 times greater than that of the relative ECSA of 1.25. The large difference between the relative mass activity and the relative ECSA would be explained by the effect of the metal–support interaction between the PtRu nanoparticles and the TECNF support.

Although we assumed an interaction between the PtRu nanoparticles and TiO_2 in order to explain the significantly high MOR activities of the PtRu/TECNF, we do not deny the possibility of the metal–support interaction not only between the PtRu nanoparticles and TiO_2, but also among the PtRu nanoparticles, TiO_2 and (N-doped) carbon. Further studies are needed to clarify the mechanism of the interaction in this system.

3.5. DMFC performance

Fig. 8 shows a comparison of the current–voltage curves between the DMFC with PtRu/TECNF[1.0] which showed the highest activity and that using the commercial PtRu/C (TEC61E54, Tanaka Kikinzoku Kogyo K.K., Pt 30.0 wt%, Ru: 23.3 wt%, denoted as PtRu/C_{com}), at 353 K, 2 M methanol (1.5 mL min^{-1}) and O_2 (1 L min^{-1}). The PtRu loadings for the anode of each DMFC were different from each other. It was 0.58 $mg_{\text{-PtRu}}$ cm^{-2} and 2.06 $mg_{\text{-PtRu}}$ cm^{-2} for PtRu/TECNF[1.0] and PtRu/C_{com}, respectively. In the figure, the DMFC with the PtRu/TECNF[1.0] showed a superior performance;

Table 3
Summary of the CO stripping voltammetry and the mass activity for the PtR/TECNF with the different Ti/C ratios.

Catalyst	CO stripping peak potential [V vs. NHE]	ECSA [m^2 ($g_{\text{-PtRu}}$)$^{-1}$]	ECSA, relative value [-]	Mass activity, relative value [-]
PtRu/TECNF[0]	0.565	342	1.00	1.00
PtRu/TECNF[0.2]	0.546	354	1.03	1.55
PtRu/TECNF[1.0]	0.516	427	1.25	2.55
PtRu/TECNF[1.9]	0.567	294	0.86	2.23
PtRu/TECNF[2.6]	0.573	296	0.87	1.00

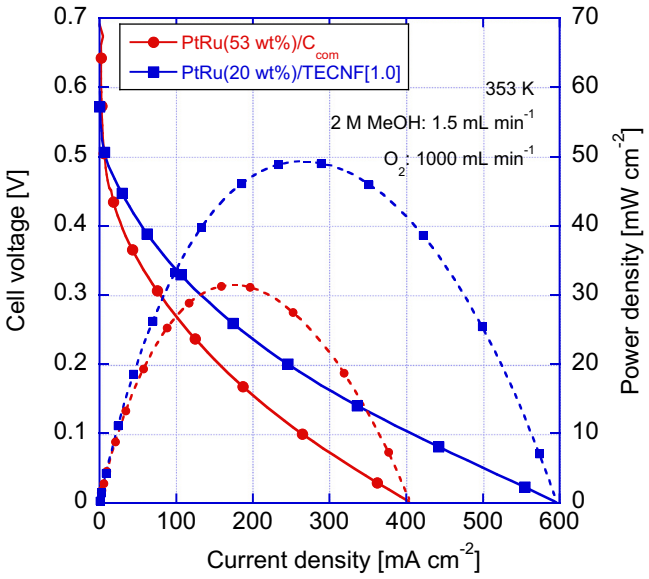

Fig. 8. Current–voltage curves for the DMFCs with PtRu/TECNF[1.0], with the PtRu loading of 0.58 $mg_{\text{-PtRu}}$ cm^{-2}, and that with the commercial PtRu/C, of which the PtRu loading was 2.06 $mg_{\text{-PtRu}}$ cm^{-2}, measured at 353 K in 2 M methanol (1.5 mL min^{-1}) and dry oxygen (1 L min^{-1}).

the max power density was 50 mW cm^{-2}, while that with the PtRu/C_{com}, the max power density was 32 mW cm^{-2}, although the amount of the PtRu loading was 1/4 that of the PtRu/C_{com}. The superior performance of the DMFC with PtRu/TECNF[1.0] could also be confirmed by comparing the performance with that in a previous study [45] that investigated the effect of the catalyst loading for the same catalyst (TEC61E54, Tanaka Kikinzoku Kogyo K.K.) and with the same operating conditions as this experiment, except for using the Nafion 112 membrane, and showed the maximum power density of 55 mW cm^{-1} for 2.7 $mg_{\text{-PtRu}}$ cm^{-2}, and 20 mW cm^{-1} for 1.0 $mg_{\text{-PtRu}}$ cm^{-2}.

Fig. 9 shows the time progress of the current density at the constant cell voltage of 0.2 V for the DMFC with the different anode catalysts, PtRu/TECNF[1.0] and PtRu/C_{com}, measured in 2 M

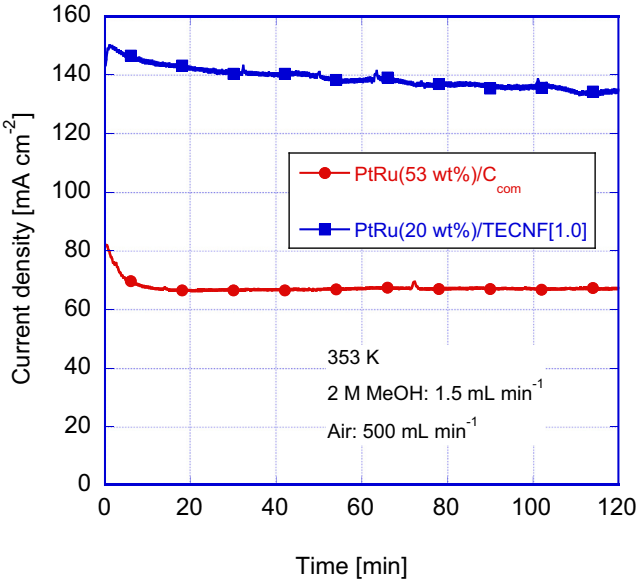

Fig. 9. Plot of current density at the constant cell voltage of 0.2 V vs. time for the DMFCs with the different anode catalysts measured at 353 K in 2 M methanol.

methanol (1.5 mL min^{-1}) and air (0.5 L min^{-1}). The lower initial current density of each DMFC, which compares with that in Fig. 8, was due to the disadvantage of using air instead of oxygen. The significantly higher power density, almost 2 times higher, was obtained for the DMFC with PtRu/TECNF[1.0] and was maintained during the experiment for over 2 h, although the amount of the PtRu loading was as low as 1/4 of the reference.

It was demonstrated that the superior DMFC performance with PtRu/TECNF[1.0] confirmed the significantly higher MOR activity of the catalyst with the TECNF support compared to the conventional PtRu/C catalyst. TECNF is a promising support for the PtRu nanocatalyst for the MOR and DMFC.

4. Conclusion

TiO_2-embedded carbon nanofibers have been prepared by electrospinning and used as a support for the anode catalyst of a DMFC. The catalyst activities of the PtRu nanoparticles prepared on different supports, i.e., Pt/C, PtRu/TiO_2, PtRu/CNF, PtRu/(C + TiO_2) and PtRu/TECNF, were compared to each other. The PtRu/TECNF showed the highest performance of the prepared catalysts, which was attributed to the metal–support interface between PtRu nanoparticles and TECNF and to the increased properties of the catalyst layer with the nanofiber catalyst. The TiO_2 content in the TECNF was sensitive to the MOR activity. The optimum Ti/C ratio in the TECNF was found to be around 1.0. PtRu/TCNF[1.0] showed a 4-times higher mass activity than PtRu/C, and a DMFC with PtRu/TECNF[1.0] generated a 2-times higher power output with 1/4 the amount of PtRu compared to a DMFC with PtRu/C_{com}. TECNF is the promising support for the PtRu nanocatalyst for the MOR and DMFC.

Acknowledgments

Part of this work was supported by the Element Innovation Project, Ministry of Education, Japan. Mohammad Ali Abdelkareem thanks JSPS for a fellowship.

References

[1] A.S. Aricò, S. Srinivasan, V. Antonucci, Fuel Cells 1 (2001) 133–161.
[2] T. Tsujiguchi, M.A. Abdelkareem, T. Kudo, N. Nakagawa, T. Shimizu, M. Matsuda, J. Power Sources 195 (2010) 5975–5979.
[3] N. Nakagawa, T. Tsujiguchi, S. Sakurai, R. Aoki, J. Power Sources 192 (2012) 325–332.
[4] B. Gurau, R. Viswanathan, R. Liu, T.J. Lafrenz, K.L. Ley, et al., J. Phys. Chem. B 102 (1998) 9997–10003.
[5] Mardwita, H. Matsune, S. Takenaka, M. Kishida, J. Chem. Eng. Jpn. 45 (2012) 493–497.
[6] M. Watanabe, S. Motoo, J. Electroanal. Chem. 60 (1975) 275–283.
[7] K.A. Friedrich, K.P. Geyzers, U. Linke, U. Stimming, J. Stumper, J. Electroanal. Chem. 402 (1996) 123–128.
[8] J.W. Guo, T.S. Zhao, J. Prabhuram, R. Chen, C.W. Wong, Electrochim. Acta 51 (2005) 754–763.
[9] M.-S. Loffler, H. Natter, R. Hempelmann, K. Wippermann, Electrochim. Acta 48 (2003) 3047–3051.
[10] Y. Shao, J. Sui, G. Yin, Y. Gao, Appl. Catal. B Environ. 79 (2008) 89–99.
[11] F. Jaouen, S. Marcotte, J. Dodelet, G. Lindbergh, J. Phys. Chem. B 107 (2003) 1376–1386.
[12] J. Prabhuram, T.S. Zhao, Z.K. Tang, R. Chen, Z.X. Liang, J. Phys. Chem. B 110 (2006) 5245–5252.
[13] P. Joghee, S. Pylypenko, T. Olson, A. Dameron, A. Gorpuz, H. Dinh, K. Wood, K. O'Neill, K. Hurst, G. Bender, T. Gennett, B. Pivovar, R. O'Hayre, J. Electrochem. Soc. 159 (2012) F768–F778.
[14] Z. Liu, X.Y. Ling, X. Su, J.Y. Lee, J. Phys. Chem. B 108 (2004) 8234–8240.
[15] G. Wu, D. Li, C. Dai, D. Wang, N. Li, Langmuir 24 (2008) 3566–3575.
[16] Y.L. Hsin, K.C. Hwang, C.-T. Yeh, J. Am. Chem. Soc. 129 (2007) 9999–10010.
[17] S. Sharma, B.G. Pollet, J. Power Sources 208 (2012) 96–119.
[18] S.-Y. Huang, P. Ganesan, S. Park, B.N. Popov, J. Am. Chem. Soc. 131 (2009) 13898–13899.
[19] A. Santasalo-Aarnio, M. Borghei, I.V. Anoshkin, A.G. Nasibulin, E.I. Kauppinen, V. Ruiz, T. Kallio, Int. J. Hydrogen Energy 37 (2012) 3415–3424.
[20] E. Formo, Z. Peng, E. Lee, X. Lu, H. Yang, Y. Xia, J. Phys. Chem. C 112 (2008) 9970–9975.
[21] Y. Zhou, K. Neyerlin, T.S. Olson, S. Pylypenko, J. Bult, H.N. Dinh, T. Gennett, Z. Shao, R. O'Hayre, Energy Environ. Sci. 3 (2010) 1437–1446.
[22] R.E. Fuentes, B.L. Garcia, J.W. Weidner, J. Electrochem. Soc. 158 (2011) B461–B466.
[23] K. Drew, G. Girishkumar, K. Vinodgopal, P.V. Kamat, J. Phys. Chem. B 109 (2005) 11851–11857.
[24] H. Songa, X. Qiu, X. Li, F. Li, W. Zhub, L. Chen, J. Power Sources 170 (2007) 50–54.
[25] L. Yu, J. Xi, Electrochim. Acta 67 (2012) 166–171.
[26] X. Zhao, J. Zhu, L. Liang, J. Liao, C. Liu, W. Xing, J. Mater. Chem. 22 (2012) 19718–19725.
[27] W. Wang, H. Wang, J. Key, V. Linkov, S. Ji, R. Wang, Ionics 19 (2013) 529–534.
[28] H.-J. Kim, D.-Y. Kim, H. Han, Y.-G. Shul, J. Power Sources 159 (2006) 484–490.
[29] K.G. Nishanth, P. Sridhar, S. Pitchumani, A.K. Shukla, ECS Trans. 41 (2011) 1139–1149.
[30] T. Miyalagan, B. Viswanathan, U.V. Varadaraju, J. Nanosci. Nanotechnol. 6 (2006) 2067–2071.
[31] S.J. Yoo, K.-S. Lee, Y.-H. Cho, S.-K. Kim, T.-H. Lim, Y.-E. Sung, Electrocatalysis 2 (2011) 297–306.
[32] M. Hepel, I. Dela, T. Hepel, J. Luo, C.J. Zhong, Electrochim. Acta 52 (2007) 5529–5547.
[33] P. Xiao, X. Guo, D.-J. Guo, H.-Q. Song, J. Sun, Z. Lv, Y. Liu, X.-P. Qiu, W.-T. Zhu, L.-Q. Chen, U. Stimming, Electrochim. Acta 58 (2011) 541–550.
[34] J. Xi, J. Wang, L. Yu, X. Qiu, L. Chen, Chem. Commun. (2007) 1656–1658.
[35] T. Ioroi, Z. Siroma, N. Fujiwara, S. Yamazaki, K. Yasuda, Electrochem. Commun. 7 (2005) 183–188.
[36] S.Lj. Gojkovic, B.M. Babic, V.R. Radmilovic, N.V. Krstajic, J. Electroanal. Chem. 639 (2010) 161–166.
[37] Q. Lv, M. Yin, X. Zhao, C. Li, C. Liu, W. Xing, J. Power Sources 218 (2012) 93–99.
[38] W.C. Conner Jr., J.L. Falconer, Chem. Rev. 95 (1995) 759–788.
[39] H. Lin, J. Mol. Catal. A Chem. 144 (1999) 189–197.
[40] J.M. Jaksic, D. Labou, G.D. Papakonstantinou, A. Siokou, M.M. Jaksic, J. Phys. Chem. C 114 (2010) 18298–18312.
[41] S. Cavaliere, S. Subuanto, I. Suvych, D.J. Jones, J. Roziere, Energy Environ. Sci. 4 (2011) 4761–4785.
[42] X. Sakai, K. Kawakami, M. Taya, J. Chem. Eng. Jpn. 45 (2012) 436–440.
[43] A.R. Corpuz, T.S. Olson, P. Joghee, S. Pylypenko, A.A. Dameron, H.N. Dinh, K.J. O'Neill, K.E. Hurst, G. Bender, T. Gennett, B.S. Pivovar, R.M. Richardes, R.P. O'Hayre, J. Power Sources 217 (2012) 142–151.
[44] C. Feng, M.A. Abdelkareem, T. Tsujiguchi, N. Nakagawa, J. Power Sources 242 (2013) 57–64.
[45] N. Nakagawa, Y. Xu, J. Power Sources 118 (2003) 248–255.